

# OLD BUT STILL WARM: FAR-UV DETECTION OF PSR B0950+08 \*

G. G. PAVLOV,<sup>1</sup> B. RANGELOV,<sup>2</sup> O. KARGALTSEV,<sup>3</sup> A. REISENEGGER,<sup>4</sup> S. GUILLOT,<sup>4</sup> AND C. REYES<sup>4</sup>

<sup>1</sup>*Pennsylvania State University, Department of Astronomy & Astrophysics, 525 Davey Lab., University Park, PA 16802; ggp1@psu.edu*

<sup>2</sup>*Texas State University, Department of Physics, 601 University Drive, San Marcos, TX 78666*

<sup>3</sup>*George Washington University, Department of Physics, 725 21st St, NW, Washington, DC 20052*

<sup>4</sup>*Instituto de Astrofísica, Pontificia Universidad Católica de Chile, Av. Vicuña Mackenna 4860, Macul, Santiago, Chile*

## ABSTRACT

We report on a *Hubble Space Telescope* detection of the nearby, old pulsar B0950+08 ( $d \simeq 262$  pc, spin-down age 17.5 Myr) in two far-ultraviolet (FUV) bands. We measured the mean flux densities  $\bar{f}_\nu = 109 \pm 6$  nJy and  $83 \pm 14$  nJy in the F125LP and F140LP filters (pivot wavelengths 1438 and 1528 Å). Using the FUV data together with previously obtained optical-UV data, we conclude that the optical-FUV spectrum consists of two components – a nonthermal (presumably magnetospheric) power-law spectrum ( $f_\nu \propto \nu^\alpha$ ) with slope  $\alpha \sim -1.2$  and a thermal spectrum emitted from the bulk of the neutron star surface with a temperature in the range of  $(1\text{--}3) \times 10^5$  K, depending on interstellar extinction and neutron star radius. These temperatures are much higher than predicted by neutron star cooling models for such an old pulsar, which means that some heating mechanisms operate in neutron stars. A plausible mechanism responsible for the high temperature of PSR B0950+08 is the interaction of vortex lines of the faster rotating neutron superfluid with the slower rotating normal matter in the inner neutron star crust (vortex creep heating).

*Keywords:* pulsars: individual (PSR B0950+08 = PSR J0953+0755) — stars: neutron — stars: ultra-violet

arXiv:1710.06448v1 [astro-ph.HE] 17 Oct 2017

\* Based on observations made with the NASA/ESA *Hubble Space Telescope*, obtained at the Space Telescope Science Institute, which is operated by the Association of Universities for Research in Astronomy, Inc., under NASA contract NAS 5-26555. These observations are associated with program #13783.

## 1. INTRODUCTION

Born extremely hot, neutron stars (NSs) lose their thermal energy via neutrino and photon emission. The cooling rate is determined by the state and composition of the NS interiors, which are still poorly known. Therefore, the study of the thermal evolution of NSs is an important tool for understanding the fundamental properties of matter. In particular, the comparison of the surface temperatures,  $T_5 \equiv T_\infty/10^5 \text{ K} = 5\text{--}20$  ( $T_\infty$  is the temperature as measured by a distant observer), of young and middle-aged ( $\tau \lesssim 1 \text{ Myr}$ ) NSs, measured in X-rays (e.g., Pavlov et al. 2002; De Luca et al. 2005) with model cooling curves  $T_\infty(\tau)$  has constrained the properties of superfluidity of the super-dense matter and perhaps even the masses of some isolated NSs (Yakovlev & Pethick 2004; Page et al. 2009).

While the cooling of young NSs in the neutrino-dominated cooling era ( $\tau \lesssim 1 \text{ Myr}$ ) has been reasonably well investigated, the thermal evolution of older NSs remains virtually unexplored. If a NS just cools passively, then its surface temperature is expected to drop very fast in the photon-dominated cooling era ( $\tau \gtrsim 1 \text{ Myr}$ ), going below  $10^4 \text{ K}$  at  $\tau \sim 10 \text{ Myr}$ . However, it has long been recognized that various heating processes may slow (or even reverse) the cooling (e.g., Gonzalez & Reisenegger 2010, and references therein). The first observational evidence of heating of old NSs was obtained by Kargaltsev et al. (2004) from *Hubble Space Telescope* (*HST*) observations of the nearest millisecond (recycled) pulsar J0437–4715, whose characteristic (spin-down) age<sup>1</sup>  $\tau_{\text{sd}} \approx 7 \text{ Gyr}$ . These authors found that its far-UV (FUV) emission is thermal, corresponding to a NS surface temperature  $T_5 \sim 1\text{--}2$ , which was later confirmed by Durant et al. (2012). This high temperature was explained by Fernández & Reisenegger (2005) as caused by “rotochemical heating” due to composition changes and accompanying non-equilibrium Urca reactions (such as neutron beta decays) forced by the density increase as the centrifugal force decreases in the course of NS spindown (Reisenegger 1995).

In addition to the rotochemical heating, other NS heating mechanisms have been proposed. For instance, “frictional heating” due to interaction of vortex lines of the faster rotating neutron superfluid with the slower rotating normal matter in the inner NS crust should be most relevant for “classical” (non-recycled) pulsars with much longer periods and stronger magnetic fields (Al-

par et al. 1984; Shibazaki & Lamb 1989; Larson & Link 1999; Gonzalez & Reisenegger 2010).

To probe the thermal evolution of old NSs, including both classical and recycled pulsars, we initiated an *HST* program #17378. First results from this program were reported by Rangelov et al. (2017) who analyzed the observations of the solitary millisecond pulsar J2124–3358 and found that its FUV emission is likely thermal, corresponding to a temperature  $T_5 \sim 0.5\text{--}2$ . Here we report the results of our observation of another target of that program, the old classical pulsar B0950+08.

PSR B0950+08 (= J0953+0755; B0950 hereafter) is a solitary radio pulsar (no  $\gamma$ -ray emission detected) with the period  $P = 253 \text{ ms}$ , spin-down energy loss rate  $\dot{E} = 5.6 \times 10^{32} \text{ erg s}^{-1}$ , spin-down age  $\tau_{\text{sd}} = 17.5 \text{ Myr}$ , and surface magnetic field  $B \sim 2.4 \times 10^{11} \text{ G}$  (Manchester et al. 2005). B0950 has a parallax distance  $d = 262 \pm 5 \text{ pc}$  and an accurately measured proper motion,  $\mu_\alpha \cos \delta = -2.09 \pm 0.08 \text{ mas yr}^{-1}$ ,  $\mu_\delta = 29.46 \pm 0.07 \text{ mas yr}^{-1}$ , corresponding to the transverse velocity  $V_\perp = 36.6 \pm 0.7 \text{ km s}^{-1}$  (Briskin et al. 2002).

X-ray emission from B0950 was barely detected with the *Einstein* IPC (Seward & Wang 1988) and *ROSAT* PSPC (Manning & Willmore 1994). Much deeper *XMM-Newton* EPIC observations of B0950 were carried out in 2002. Becker et al. (2004) described the phase-integrated X-ray spectrum with an absorbed power-law (PL) model ( $f_E \propto E^{1-\Gamma}$ , where  $f_E$  is the energy flux density) with photon index  $\Gamma = 1.92_{-0.12}^{+0.14}$ , absorbing hydrogen column density  $N_{H,20} \equiv N_H/(10^{20} \text{ cm}^{-2}) = 2.6_{-2.4}^{+2.7}$ , and unabsorbed flux  $F_{0.5-10 \text{ keV}}^{\text{unabs}} = 8.7_{-0.9}^{+1.0} \times 10^{-14} \text{ erg cm}^{-2} \text{ s}^{-1}$ , corresponding to the luminosity<sup>2</sup>  $L_{0.5-10 \text{ keV}} = 7.1_{-0.7}^{+0.9} \times 10^{29} \text{ erg s}^{-1}$ . These authors also reported pulsations with one and two peaks per period in the 2–10 and 0.3–2 keV bands, respectively. Zavlin & Pavlov (2004) suggested that the additional peak at lower energies can be explained by the contribution of thermal polar cap emission. They interpreted the same data as a combination of nonthermal (presumably magnetospheric) emission with a PL spectrum ( $\Gamma = 1.3 \pm 0.1$ ,  $L_{0.2-10 \text{ keV}} = (1.0 \pm 0.1) \times 10^{30} \text{ erg s}^{-1}$ ) and thermal emission from heated polar caps covered with a hydrogen atmosphere, which dominates at  $E \lesssim 0.7 \text{ keV}$ . Using hydrogen atmosphere models (Pavlov et al. 1995), they estimated the effective temperature, radius, and bolometric luminosity of polar caps:  $T_{\text{pc}} \approx 1 \text{ MK}$ ,

<sup>1</sup> Since the true ages of old pulsars are unknown, their spin-down ages,  $\tau_{\text{sd}} \equiv P/(2\dot{P})$ , are commonly used as age estimates.

<sup>2</sup> This luminosity value is estimated as  $L = 4\pi d^2 F_{\text{unabs}}$ , with  $d = 262 \text{ pc}$ , as well as other luminosities in this paper. The luminosity quoted by Becker et al. (2004) is a factor of 4 lower.

$R_{\text{pc}} \approx 250 \text{ m}$ ,  $L_{\text{pc}} \approx 3 \times 10^{29} \text{ erg s}^{-1}$ , at the hydrogen column density restricted to the range  $2 < N_{\text{H},20} < 4$ .

Optical-UV emission from B0950 was discovered by Pavlov et al. (1996) in *HST* observations with the Faint Object Camera (FOC) in a long-pass filter F130LP (pivot wavelength  $3438 \text{ \AA}$ ,  $\text{FWHM} \approx 2000 \text{ \AA}$ ). They measured a mean spectral flux density  $\bar{f}_\nu = 51 \pm 3 \text{ nJy}$  in this filter. Pavlov et al. (1996) considered the possibility that this could be, at least partly, thermal emission from the entire NS surface, which gives an upper limit  $T_5 \lesssim 3$  on the brightness temperature (for the apparent NS radius  $R_\infty = 13 \text{ km}$ , the modern distance estimate,  $d = 262 \text{ pc}$ , and negligibly low interstellar extinction).

Observations with the Subaru telescope allowed Zharikov et al. (2002) to measure the flux density of  $60 \pm 9 \text{ nJy}$  in the B filter. Observations with the VLT/FORS1 telescope (Zharikov et al. 2004) gave the B, V, R and I flux densities of  $60 \pm 17$ ,  $45 \pm 6$ ,  $91 \pm 8$  and  $78 \pm 11 \text{ nJy}$ , respectively. Despite the large scatter of the flux values (likely caused by a contamination, particularly in the I and R bands, from a very red, possibly extended object at about  $1''$  north of the pulsar; see Figure 2 in Zharikov et al. 2004), it is clear that the optical emission from B0950 is nonthermal. Fitting these flux densities with a PL model, Zharikov et al. (2004) obtained a spectral slope  $\alpha = -0.65 \pm 0.40$  ( $f_\nu \propto \nu^\alpha$ ,  $\alpha = 1 - \Gamma$ ). Figure 3 of that paper suggests that the earlier detected emission in the F130LP filter was mostly nonthermal, although some contribution from a thermal component could not be excluded. Zavlin & Pavlov (2004) have shown that the VLT/FORS1 spectrum and the nonthermal component of the X-ray spectrum are consistent with a single PL model, with  $\Gamma \approx 1.3\text{--}1.4$ . For this model, the broadband nonthermal luminosity is  $L_{1\text{eV--}10\text{keV}}^{\text{nonth}} = 1.1 \times 10^{30} \text{ erg s}^{-1} = 1.8 \times 10^{-3} \dot{E}$ , of which the optical luminosity is a small fraction (e.g.,  $L_{1\text{--}5\text{eV}} = 5.2 \times 10^{27} \text{ erg s}^{-1} = 4.7 \times 10^{-3} L_{1\text{eV--}10\text{keV}}^{\text{nonth}}$ ). Using this interpretation, Zavlin & Pavlov (2004) suggested an upper limit on the brightness temperature in the optical-UV:  $T_5 \lesssim 1.5$ , for  $R_\infty = 13 \text{ km}$ ,  $\alpha = -0.35$ , and reddening  $E(B - V) = 0.05$ .

Thus, it still remains unclear how hot is the bulk of the B0950 NS surface. To measure or constrain it, we observed this pulsar in the FUV with the *HST*.

## 2. OBSERVATIONS

B0950 was observed with the Solar-Blind Channel (SBC) of the Advanced Camera for Surveys (ACS) in two visits that occurred on 2016 January 29 (one orbit) and 2016 February 4 (two orbits). We split the observations in two visits (see Table 1) to reduce the instrumental background (“thermal glow”, caused by heat-

ing of the detector), which rises dramatically with the length of time the detector is turned on<sup>3</sup>. The SBC has a nominal field of view  $\approx 34'' \times 30''$ . During each orbit the data were taken in long-pass filters F125LP and F140LP, with pivot wavelengths  $1438$  and  $1528 \text{ \AA}$ , respectively (see Figure 1). The F125LP images were taken in the Earth shadow to minimize the geocoronal FUV background. The F140LP filter, which cuts off bright geocoronal oxygen lines, was used in non-shadow parts of the orbit.

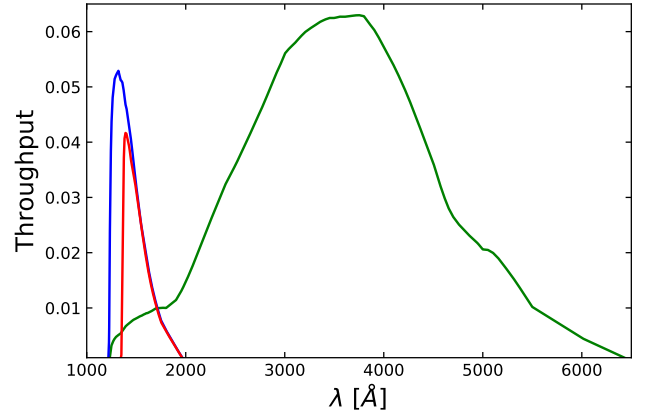


**Figure 1.** Throughputs of the *HST* filters SBC/F125LP (blue), SBC/F140LP (red) and FOC/F130LP (green) used in the observations of B0950.

## 3. DATA ANALYSIS AND RESULTS

For the data analysis, we used the pipeline-calibrated data files stored the Mikulski Archive for Space Telescopes (MAST<sup>4</sup>). The MAST images are coaligned and corrected for geometric distortion using the DrizzlePac *AstroDrizzle* task<sup>5</sup>.

### 3.1. FUV images

Figure 2 shows SBC/F125LP images of the B0950 field obtained in the two visits. In each of the images we see a point-like source<sup>6</sup> near the image center and two extended objects, presumably galaxies. We also see that

<sup>3</sup> See [http://www.stsci.edu/hst/acs/documents/handbooks/current/c04\\_detector6.html#325708](http://www.stsci.edu/hst/acs/documents/handbooks/current/c04_detector6.html#325708).

<sup>4</sup> See <http://archive.stsci.edu/>

<sup>5</sup> <http://drizzlepac.stsci.edu/>

<sup>6</sup> Zoomed-in images of the source obtained in separate visits show asymmetric extensions with lengths  $\lesssim 0''.2$  (see insets in Figure 2). Since the directions of these extensions are different in different orbits, we conclude that they are due to instrumental effects.

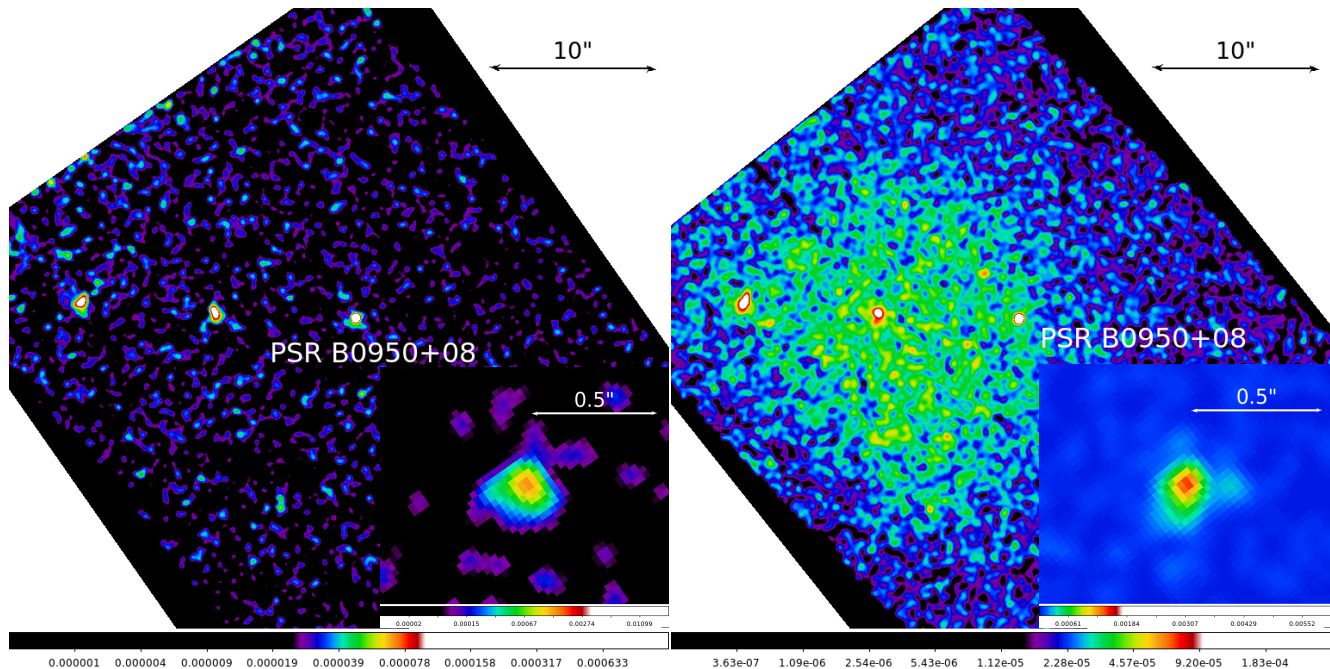


**Figure 2.** SBC/F125LP images of B0950 and its surroundings for Visit 1 (one *HST* orbit; left) and Visit 2 (two orbits; right), smoothed with a  $0.1''$  width Gaussian. North is up, East to the left. The diffuse “emission” in the Visit 2 image is the instrumental “thermal glow” caused by detector heating during the second orbit of that visit. The  $\approx 1.2'' \times 1.0''$  insets show the zoomed-in images of the pulsar and its immediate vicinity.

the SBC thermal glow background, indiscernible in the one-orbit Visit 1, is much brighter in the two-orbit Visit 2 because the detector became hotter in the second orbit of this visit.

The nominal coordinates of the point source in the MAST images are  $\alpha = 09:53:09.347$ ,  $\delta = 07:55:35.79$  in Visit 1 and  $\alpha = 09:53:09.343$ ,  $\delta = 07:55:35.74$  in Visit 2 (centroiding uncertainty about a few times  $0.01''$ ). The corresponding source positions differ by  $1.05''$  and  $1.06''$  from the expected radio pulsar position,  $\alpha = 09:53:09.3054(19)$ ,  $\delta = 07:55:36.64(8)$ , at the time of observation (MJD 57419). Such offsets, due to telescope pointing errors, are not unusual in *HST* observations<sup>7</sup>. In addition, no field objects were seen in the pulsar vicinity in the deep *HST* FOC/F130LP and Subaru B-filter observations. Moreover, the optical-UV spectrum of the candidate pulsar counterpart (see below) is quite unusual for a field star but natural for a pulsar. It means that the detected object is indeed an FUV counterpart of B0950.

We know from the VLT observations that there is a background object (likely a distant galaxy) very close to the B0950 position,  $\approx 0.9''$  from the pulsar in 2001 January (Zharikov et al. 2004). Its expected distance from the pulsar became  $\approx 0.4''$ – $0.5''$  by the time of our observations (assuming the object’s proper motion is negligible). However, this object is very faint and extremely red (not seen by Subaru and VLT in the B band). Therefore, it should not make any contribution in FUV.

### 3.2. Photometry

For the pulsar photometry, we used “drizzled” MAST images for each of the visits, and the Python aperture photometry tool *Photutils*. The pixel scale in the drizzled images is  $0.025''$ . To find the optimal source aperture, we calculated the signal-to-noise ratio ( $S/N$ ) as a function of radius of circular aperture centered on the brightest pixel. For the F125LP images, we chose the  $r = 10$  pixels source aperture which provides  $S/N \approx 10$  and 14 for Visit 1 and Visit 2, respectively. We extracted the background from an annulus with the inner and outer radii of 30 and 70 pixels (area  $A_b = 7.854$  arcsec<sup>2</sup>). For the shallow F140LP images, the  $S/N$  dependence on  $r$  is rather noisy, but the same  $r = 10$  pixels

<sup>7</sup> See, e.g., <http://www.stsci.edu/hst/acs/documents/isrs/isr0506.pdf>



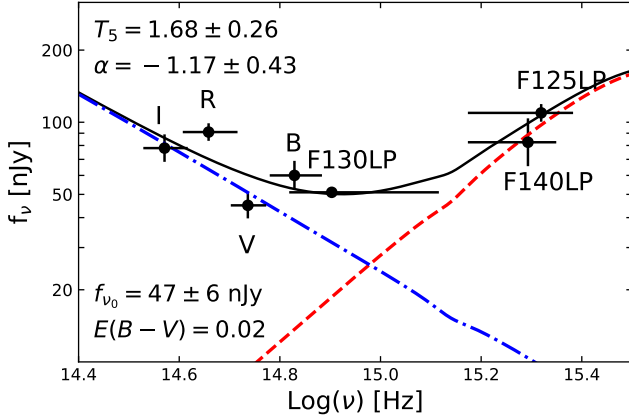


**Figure 3.** Spectral fit for the *HST* (F125LP, F140LP, F130LP), Subaru (B) and VLT (V, R, I) data with the PL+BB model for  $E(B - V) = 0.02$ ,  $R_{12}/d_{262} = 1$ . The horizontal bars show the filter widths at half maxima of their throughputs, the mean flux values are plotted at the pivot frequencies of the filters.

source aperture provides  $S/N \approx 3.7$  and 4.6 (for Visits 1 and 2) close to their maximum values.

Using the numbers of counts,  $N_t$  and  $N_b$ , in the source and background apertures (see Table 1), we calculated the number of source counts,  $N_s = N_t - (A_s/A_b)N_b$ , and its uncertainty,  $\delta N_s = [N_t + (A_s/A_b)^2 N_b]^{1/2}$ , for each of the filters and visits. We corrected the corresponding count rates for the finite aperture size using the encircled energy fractions of 0.66 and 0.665 for the F125LP and F140LP filters, respectively<sup>8</sup>.

We used the aperture-corrected count rates,  $C_s$  in Table 1, to calculate the mean flux densities,

$$\bar{f}_\nu \equiv \left[ \int f_\nu T(\nu) \nu^{-1} d\nu \right] \left[ \int T(\nu) \nu^{-1} d\nu \right]^{-1} = \mathcal{P}_\nu C_s, \quad (1)$$

where  $f_\nu$  is the energy flux density,  $T(\nu)$  is the filter throughput as a function of frequency, and  $\mathcal{P}_\nu$  is the conversion factor<sup>9</sup> ( $\mathcal{P}_\nu = 1.19$  and  $2.12$  nJy ks cnt<sup>-1</sup> for the F125LP and F140LP filters, respectively).

<sup>8</sup> The encircled energy fractions were calculated using Table 2 in the Instrument Science Report ACS 2016-05 by Avila & Chiaberge, <http://www.stsci.edu/hst/acs/documents/isrs/isr1605.pdf>. The aperture size is sufficiently large to neglect the effect of the artificial “extensions” of the pulsar image (see footnote 6 and Figure 2) on the encircled energy fraction.

<sup>9</sup> Note that  $\mathcal{P}_\nu$  (and hence the  $\bar{f}_\nu$  value for a given  $C_s$ ) do not depend on the shape of  $f_\nu$ . In a similar manner, one can define  $\bar{f}_\lambda = \mathcal{P}_\lambda C_s$ , where  $\mathcal{P}_\lambda = \mathcal{P}_\nu c \lambda_{\text{piv}}^{-2}$  (‘photflam’ header keyword in calibrated *HST* data),  $\lambda_{\text{piv}}^2 = [\int T(\lambda) \lambda d\lambda] [\int T(\lambda) \lambda^{-1} d\lambda]^{-1}$  is the pivot wavelength squared.

### 3.3. Spectral fits

We used our photometry results and the previous *HST*, Subaru and VLT observations (Pavlov et al. 1996; Zharikov et al. 2002, 2004) to fit model spectra to the data. Contrary to the VLT optical spectrum, the overall broadband spectrum in the 1250–9000 Å range (see, e.g., Figure 3) cannot be described by a single PL model because of the relatively high FUV flux (e.g., at  $E(B - V) = 0.02$  the best-fit PL model,  $\alpha = +0.4 \pm 0.3$ , corresponds to an unacceptably large reduced  $\chi_\nu^2 = 10.6$  for 5 degrees of freedom [dof]). The FUV excess can be naturally interpreted as thermal emission from the NS surface. Therefore, we fit the data with a two-component PL+blackbody (BB) model (see, e.g., Pavlov et al. 1997; Kargaltsev & Pavlov 2007):

$$f_\nu = \left[ f_{\nu_0} \left( \frac{\nu}{\nu_0} \right)^\alpha + \frac{R_\infty^2}{d^2} \pi B_\nu(T_\infty) \right] \times 10^{-0.4A_\nu}, \quad (2)$$

where  $\nu_0$  is the reference frequency (we chose  $\nu_0 = 6 \times 10^{14}$  Hz),  $d = 262d_{262}$  pc is the distance,  $B_\nu(T_\infty) = (2h\nu^3/c^2)[\exp(h\nu/kT_\infty) - 1]^{-1}$  is the Planck function, the temperature  $T_\infty = 10^5 T_5$  K and the radius  $R_\infty = 12R_{12}$  km are as measured by a distant observer.

The extinction coefficient  $A_\nu$  is proportional to the color excess  $E(B - V)$  (dust reddening), which can be crudely estimated using the hydrogen column density:  $E(B - V) = (0.0146 \pm 0.0006) N_{H,20}$  mag (e.g., Güver & Özel 2009). The  $N_H$  values obtained from X-ray spectral fits,  $N_{H,20} \sim 1$ –4, are rather uncertain; they correspond to  $E(B - V) \sim 0.014$ –0.06. The correlation between  $N_H$  and pulsar dispersion measure,  $N_{H,20} = 0.30_{-0.09}^{+0.13}$  DM (He et al. 2013), gives  $N_{H,20} \approx 0.6$ –1.3,  $E(B - V) \approx 0.01$ –0.02 (DM = 2.97 pc cm<sup>-3</sup> for B0950). The color excess can also be estimated from 3D reddening maps<sup>10</sup>:  $E(B - V) = 0.015 \pm 0.008$  and  $E(B - V) = 0.004$ –0.030 in the maps described by Lallement et al. (2014) and Green et al. (2015), respectively. Thus, a plausible range of the color excess is  $E(B - V) = 0.01$ –0.03, but higher values, up to 0.06, are not firmly excluded. We will explore the conservative range,  $E(B - V) = 0.01$ –0.06 in our fits, using the extinction curve ‘Milky Way’ from Table 3 by Clayton et al. (2003) to calculate the extinction  $A_\nu$ .

The model given by Equation (2) has 5 parameters:  $f_{\nu_0}$ ,  $\alpha$ ,  $R_\infty/d$ ,  $T_\infty$ , and  $E(B - V)$ . Because of the small number of data points and a correlation between the parameters, we have to fix some of them to obtain constrained fits. We chose to fit  $f_{\nu_0}$ ,  $\alpha$ , and  $T_\infty$  at fixed values of  $E(B - V)$  and  $R_\infty/d = 1.48 \times 10^{-15} R_{12}/d_{262}$ . An

<sup>10</sup> See <http://stilism.obspm.fr/> and <http://argonaut.skymaps.info/>

**Table 1.** Photometry of PSR B0950+08

Filter	Visit	$t_{\text{exp}}^a$	$N_t^b$	$N_b^c$	$N_s^d$	$C_s^e$	$\bar{f}_\nu^f$
		ks	cnts	cnts	cnts	cnts ks $^{-1}$	nJy
F125LP	1	1.836	114	477	102	$84.3 \pm 8.8$	$100 \pm 11$
F125LP	2	3.692	268	1382	233	$95.8 \pm 6.7$	$114 \pm 8$
F125LP	1+2	5.528	382	1859	336	$92.0 \pm 5.4$	$109.4 \pm 6.4$
F140LP	1	0.592	19	110	16.2	$41.5 \pm 11.1$	$88 \pm 24$
F140LP	2	1.182	43	532	29.8	$38.2 \pm 8.3$	$81 \pm 18$
F140LP	1+2	1.774	62	642	46.0	$39.0 \pm 6.7$	$83 \pm 14$

<sup>a</sup>Exposure time.<sup>b</sup>Total number of counts in the  $A_s = 0.196$  arcsec $^2$  source aperture.<sup>c</sup>Background counts in the  $A_b = 7.854$  arcsec $^2$  annulus.<sup>d</sup>Net source counts in the  $A_s = 0.196$  arcsec $^2$  aperture.<sup>e</sup>Aperture-corrected source count rate.<sup>f</sup>Mean flux density of the source (see text).

example of such a fit at plausible values of  $E(B - V) = 0.02$  and  $R_{12}/d_{262} = 1$  is shown in Figure 3. We see from Figure 3 that the PL component gives the main contribution to the optical flux, while the FUV flux is determined by the BB component with  $T_5 = 1.68 \pm 0.26$  and bolometric luminosity  $L_{\text{bol}}^\infty = 8.2_{-4.0}^{+6.4} \times 10^{29}$  erg s $^{-1}$ . The quality of this fit (and of the fits at other  $E(B - V)$  and  $R_\infty/d$  values) is poor (reduced  $\chi_\nu^2 = 3.8$  at 4 dof) because of the large scatter of the optical (Subaru and VLT) fluxes, likely caused by large systematic errors in correcting for the contribution of the nearby red object (see Figure 2 in Zharikov et al. 2004 and Section 1), unaccounted in the flux uncertainties. The PL normalization,  $f_{\nu_0} = 47 \pm 6$  nJy, and particularly the slope,  $\alpha = -1.17 \pm 0.43$ , are rather uncertain, due to the same reason. The slope is steeper than that obtained by Zharikov et al. (2004),  $\alpha = -0.65 \pm 0.40$ , because those authors did not include the thermal component, which gives a considerable contribution to the F130LP flux in our fits.

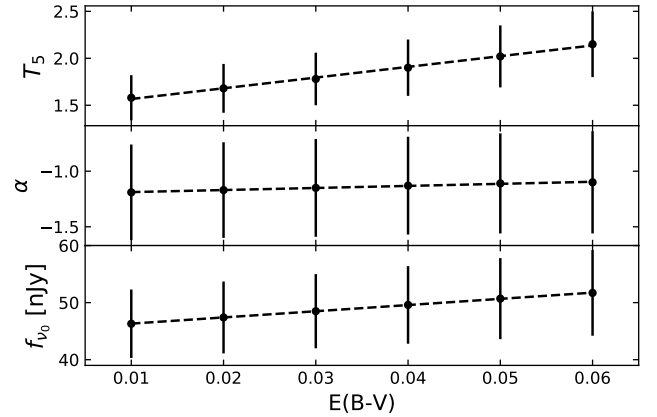
The dependences of  $T_5$ ,  $\alpha$  and  $f_{\nu_0}$  on the reddening  $E(B - V)$  for  $R_{12}/d_{262} = 1$  are shown in Figure 4. They can be approximated by linear functions:

$$T_5 = 1.45 \pm 0.22 + (11.4 \pm 2.16) E(B - V), \quad (3)$$

$$\alpha = -1.21 \pm 0.42 + (1.8 \pm 0.6) E(B - V), \quad (4)$$

$$f_{\nu_0} = [45.2 \pm 5.7 + (108 \pm 29) E(B - V)] \text{ nJy}. \quad (5)$$

We see from Figure 4 that, for the chosen  $R_{12}/d_{262} = 1$  and  $E(B - V) = 0.01$ – $0.06$ , a conservative range for the

**Figure 4.** Dependences of the fitting parameters on color excess and their linear approximations (see Equations (3)–(5)), for  $R_{12}/d_{263} = 1$ .

BB temperature is  $1.3 \lesssim T_5 \lesssim 2.5$  ( $1.3 \lesssim T_5 \lesssim 2.1$  for a more plausible extinction range  $E(B - V) = 0.01$ – $0.03$ ).

An additional uncertainty of the fitting parameters is caused by the uncertainty of the  $R_\infty/d$  ratio (mostly due to uncertain NS radius). Similar fits for a few  $R_{12}/d_{262}$  values from the plausible range  $0.9 < R_{12}/d_{262} < 1.2$  show that the best-fit temperature and its upper and

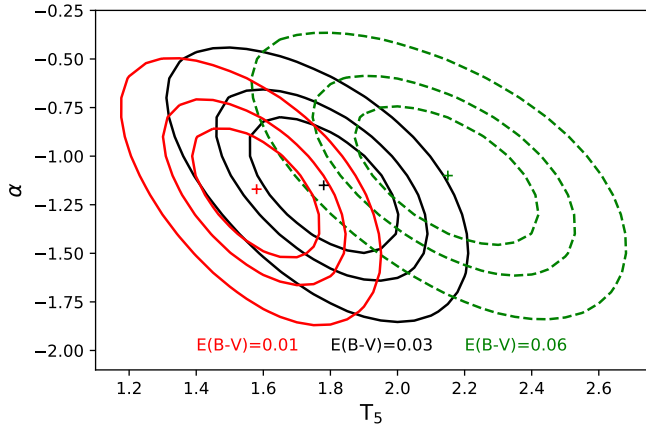


**Figure 5.** Confidence contours in the  $T_\infty$ - $\alpha$  plane for  $R_{12}/d_{262} = 1$  and three values of  $E(B-V)$ . The contours are lines of constant values of  $\chi^2_{\min} + \Delta\chi^2$ , where  $\chi^2_{\min}$  is the minimum value of  $\chi^2$  at a given  $E(B-V)$ , and  $\Delta\chi^2 = 2.3, 4.6$ , and  $9.2$  for the 68%, 90%, and 99% confidence levels, respectively, for two parameters of interest. The third parameter,  $f_{\nu_0}$ , was varied to minimize  $\chi^2$  at each point of the  $T_\infty$ - $\alpha$  grid. The solid red and black contours correspond to the minimum and maximum values of the most plausible range of the color excess,  $E(B-V) = 0.01$  and  $0.03$ , respectively; the dashed green contours correspond to the conservative upper limit,  $E(B-V) = 0.06$ .

lower bounds are proportional to<sup>11</sup>  $(R_{12}/d_{262})^{-1.5}$ , and the most conservative range of temperatures is  $1.0 \lesssim T_5 \lesssim 3.5$  ( $1.0 \lesssim T_5 \lesssim 3.0$  for the more plausible range of color excess). The temperature range is rather broad, but we stress that because of the  $T$ - $\alpha$  anti-correlation and the large uncertainty of  $\alpha$  in the current fits (see Figures 4 and 5), much more stringent constraints on  $T$  could be obtained after more accurate measurements of NIR-optical fluxes, which would require observations with high angular resolution.

Additional constraints on the temperature upper limit could be obtained from the X-ray data, but this limit depends on the interpretation of the X-ray emission, which is still controversial. For instance, assuming that the 0.3–10 keV spectrum is an absorbed PL, we found  $3\sigma$  upper limits  $T_5 < 3.1$  and  $T_5 < 3.3$  at  $N_{H,20} = 2$  and  $N_{H,20} = 4$ , respectively (for  $R_\infty = 13$  km). These limits are close to the upper bound on the temperature range obtained from the FUV-optical data. Assuming that the X-ray spectrum includes both the magnetospheric (PL)

<sup>11</sup> This dependence is weaker than  $T \propto (R_\infty/d)^{-2}$ , expected for the case when all the other parameters are fixed, because  $\alpha$  becomes more negative with increasing  $R_\infty/d$ , which results in higher fitting temperatures (see Figure 5).

component and the thermal component emitted by polar caps covered with hydrogen atmosphere, [Zavlin & Pavlov \(2004\)](#) obtained a lower value of the upper limit,  $T_5 < 1.5$ , for  $R_\infty = 13$  km,  $E(B-V) = 0.05$ . However, this model-dependent estimate was obtained assuming a constant slope of the optical through X-ray spectrum,  $\alpha = -0.35$ , much more gradual than  $\alpha = -1.12 \pm 0.45$  obtained in our FUV-optical fits at the same  $E(B-V)$ . In addition, the polar cap contribution and hence that upper limit depend on the poorly known orientation of the pulsar’s spin axis and the magnetic axis inclination as well as on the mass-to-radius ratio. These quantities could be more accurately estimated from phase-resolved spectral analysis of data obtained from a deeper X-ray observation, which would also be useful to establish the nature of the X-ray emission.

### 3.4. Upper limit on extended emission in pulsar vicinity

Although old and not very powerful, B0950 should emit a pulsar wind and be accompanied by a pulsar wind nebula (PWN). Its radiation could be emitted by shocked relativistic wind and/or shocked interstellar medium (ISM). Although FUV is not a wavelength range in which PWNe are usually looked for, the recent detections of FUV bow shocks from the millisecond pulsars J0437–4715 ([Rangelov et al. 2016](#)) and J2124–3358 ([Rangelov et al. 2017](#)) suggest that FUV PWNe could be detected from other nearby pulsars. Therefore, we looked for extended emission in the vicinity of B0950.

A characteristic PWN size can be estimated by balancing the PW pressure with the pressure exerted by the ambient ISM, including the ram pressure caused by the pulsar motion (see, e.g., Equation (1.1) in [Kargaltsev et al. 2017](#)). In the case of B0950 the characteristic size can vary from a few tenths of arc second to a few arc seconds, depending on the local ISM properties and the pulsar velocity. Inspection of our FUV images did not show extended emission around the pulsar. We measured the upper limit on its surface brightness (specific intensity) by sampling the background counts from 13 different circular regions with  $r = 1''$  within  $10''$  from the pulsar, calculating the standard deviation from the mean value and converting it to the mean flux upper limit. In the F125LP low-background image of Visit 1 we found a standard deviation of  $21.9$  counts  $\text{ks}^{-1}$  for the count rate in the  $r = 1''$  circles. It translates into a  $3\sigma$  upper limit of  $8.3$  nJy  $\text{arcsec}^{-2}$  for the specific intensity.

## 4. DISCUSSION

Our FUV observations of B0950, analyzed together with the previous optical-UV observations, have shown

that its optical radiation is nonthermal (presumably emitted from the pulsar magnetosphere) while the FUV radiation is predominantly thermal, most likely emitted from the bulk of the NS surface. The discovery of the thermal emission from the  $\sim 20$  Myr old pulsar with the brightness temperature substantially higher than predicted by the NS cooling theories is the main finding of this work.

The estimated temperature of B0950,  $T_5 = 1-3$ , is similar to those found for the millisecond pulsars J0437–4715 (Kargaltsev et al. 2004; Durant et al. 2012; Guillot et al. 2016) and J2124–3358 (Rangelov et al. 2017), hereafter J0437 and J2124. However, B0950 is a classical (non-recycled) pulsar, with a much longer rotation period, a stronger magnetic field, and a younger spin-down age, though substantially older than middle-aged ( $\tau \sim 0.1-1$  Myr) NSs whose temperatures are generally compatible with the predictions of standard cooling mechanisms.

Gonzalez & Reisenegger (2010) analyzed various possible heating mechanisms for old NSs, finding that vortex creep and rotochemical heating by non-equilibrium Urca reactions in the NS core were the only ones that could plausibly explain the fairly high temperature of J0437<sup>12</sup>. The lower panels of Figures 4 and 5 in Gonzalez & Reisenegger (2010) show the expected thermal evolution of classical pulsars with a magnetic field  $B = 2.5 \times 10^{11}$  G (nearly identical to that of B0950) for these two heating mechanisms, and the observational upper limits for several pulsars. From those plots, we infer that the estimated temperature range for B0950 is roughly consistent with their curves for vortex creep heating with either modified or direct Urca cooling, where the “excess angular momentum” parameter  $J = 5.5 \times 10^{43}$  erg s was chosen as the smallest compatible with the temperature measurement of J0437, which is also consistent with J2124. On the other hand, to explain the temperature of B0950 with rotochemical heating, we would need to invoke pure modified Urca reactions and an implausibly short initial rotation period ( $P_0 \lesssim 10$  ms), in order to allow the pulsar to accumulate a large enough chemical imbalance by its current age. UV observations of other old classical pulsars, supplemented by deep optical and X-ray observations, would allow one to firmly establish the heating mechanism and take it into account in the models of thermal evolution of NSs.

Regarding the PL optical spectrum, we note that if its slope is as steep as found from our fits,  $\alpha \approx -1.2 \pm 0.5$ ,

then the extrapolation of the optical PL to higher energies underpredicts the X-ray flux, requiring a “double break” in the optical through X-ray spectrum. Such behavior is similar to that observed in the middle-aged pulsar B1055–52 (see Figure 3 in Mignani et al. 2010), but it is unusual for pulsars detected in both the X-ray and optical ranges, for which the extrapolated optical spectrum either overpredicts or matches the X-ray spectrum (Kargaltsev & Pavlov 2007). The steep optical spectrum of B0950 might suggest that different populations of relativistic particles are responsible for the optical and X-ray nonthermal emission, but the estimated slope of the optical emission suffers from large systematic uncertainties. To measure the slope of the optical component more accurately, the pulsar should be resolved from the nearby extended optical source, presumably a distant galaxy. High-resolution observations in a few NIR-optical filters would not only determine the slope of the pulsar’s optical spectrum but would also allow one to measure the NS surface temperature more accurately than it was possible with the data available.

The detection of thermal emission from B0950, J0437, and J2124, as well as the discovery of FUV bow shocks around J0437 and J2124, demonstrate the great potential of UV observations of nearby pulsars. Earlier UV-optical observations of another type of NSs, the so-called Thermally Emitting Isolated NSs, whose emission is powered by the heat stored in the NS interiors rather than by the loss of their rotational energy, also showed a number of unexpected, not fully understood properties (Kaplan et al. 2011; Ertan et al. 2017). It would be very important to employ the unique UV capabilities of the *HST* for the study of a larger sample of isolated NSs of various types.

Support for program #13783 was provided by NASA through a grant from the Space Telescope Science Institute, which is operated by the Association of Universities for Research in Astronomy, Inc., under NASA contract NAS 5-26555. The work of AR and CR is supported by FONDECYT Regular Project 1150411, and that of SG by FONDECYT Postdoctoral Project 3150428. We are grateful to Roberto Avila for very useful consultations on the ACS SBC detector properties. We also thank Marten van Kerkwijk and Denis González-Caniulef for valuable help in preparation of the observational proposal.

*Facility:* HST(ACS)

*Software:* DrizzlePac (<http://drizzlepac.stsci.edu/>), Photutils

<sup>12</sup> A variant of rotochemical heating through pycnonuclear reactions in the NS crust was later shown to be similarly effective for millisecond pulsars (Gusakov et al. 2015).



## REFERENCES

- Alpar, M. A., Pines, D., Anderson, P. W., & Shaham, J. 1984, *ApJ*, 276, 325
- Becker, W., Weisskopf, M. C., Tennant, A. F., et al. 2004, *ApJ*, 615, 908
- Briskin, W. F., Benson, J. M., Goss, W. M., & Thorsett, S. E. 2002, *ApJ*, 571, 906
- Clayton, G. C., Wolff, M. J., Sofia, U. J., Gordon, K. D., & Misselt, K. A. 2003, *ApJ*, 588, 871
- De Luca, A., Caraveo, P. A., Mereghetti, S., Negroni, M., & Bignami, G. F. 2005, *ApJ*, 623, 1051
- Durant, M., Kargaltsev, O., Pavlov, G. G., et al. 2012, *ApJ*, 746, 6
- Ertan, Ü., Çalışkan, Ş., & Alpar, M. A. 2017, *MNRAS*, 470, 1253
- Fernández, R., & Reisenegger, A. 2005, *ApJ*, 625, 291
- Gonzalez, D., & Reisenegger, A. 2010, *A&A*, 522, A16
- Green, G. M., Schlafly, E. F., Finkbeiner, D. P., et al. 2015, *ApJ*, 810, 25
- Guillot, S., Kaspi, V. M., Archibald, R. F., et al. 2016, *MNRAS*, 463, 2612
- Gusakov, M. E., Kantor, E. M., & Reisenegger, A. 2015, *MNRAS*, 453, L36
- Güver, T., & Özel, F. 2009, *MNRAS*, 400, 2050
- He, C., Ng, C.-Y., & Kaspi, V. M. 2013, *ApJ*, 768, 64
- Kaplan, D. L., Kamble, A., van Kerkwijk, M. H., & Ho, W. C. G. 2011, *ApJ*, 736, 117
- Kargaltsev, O., & Pavlov, G. 2007, *Ap&SS*, 308, 287
- Kargaltsev, O., Pavlov, G. G., Klingler, N., & Rangelov, B. 2017, *ArXiv e-prints*, arXiv:1708.00456
- Kargaltsev, O., Pavlov, G. G., & Romani, R. W. 2004, *ApJ*, 602, 327
- Lallement, R., Vergely, J.-L., Valette, B., et al. 2014, *A&A*, 561, A91
- Larson, M. B., & Link, B. 1999, *ApJ*, 521, 271
- Manchester, R. N., Hobbs, G. B., Teoh, A., & Hobbs, M. 2005, *AJ*, 129, 1993
- Manning, R. A., & Willmore, A. P. 1994, *MNRAS*, 266, 635
- Mignani, R. P., Pavlov, G. G., & Kargaltsev, O. 2010, *ApJ*, 720, 1635
- Page, D., Lattimer, J. M., Prakash, M., & Steiner, A. W. 2009, *ApJ*, 707, 1131
- Pavlov, G. G., Shibano, Y. A., Zavlin, V. E., & Meyer, R. D. 1995, in *NATO Advanced Science Institutes (ASI) Series C*, Vol. 450, *NATO Advanced Science Institutes (ASI) Series C*, ed. M. A. Alpar, U. Kiziloglu, & J. van Paradijs, 71
- Pavlov, G. G., Stringfellow, G. S., & Cordova, F. A. 1996, *ApJ*, 467, 370
- Pavlov, G. G., Welty, A. D., & Córdoba, F. A. 1997, *ApJL*, 489, L75
- Pavlov, G. G., Zavlin, V. E., & Sanwal, D. 2002, in *Neutron Stars, Pulsars, and Supernova Remnants*, ed. W. Becker, H. Lesch, & J. Trümper, 273
- Rangelov, B., Pavlov, G. G., Kargaltsev, O., et al. 2016, *ApJ*, 831, 129
- . 2017, *ApJ*, 835, 264
- Reisenegger, A. 1995, *ApJ*, 442, 749
- Seward, F. D., & Wang, Z.-R. 1988, *ApJ*, 332, 199
- Shibasaki, N., & Lamb, F. K. 1989, *ApJ*, 346, 808
- Yakovlev, D. G., & Pethick, C. J. 2004, *ARA&A*, 42, 169
- Zavlin, V. E., & Pavlov, G. G. 2004, *ApJ*, 616, 452
- Zharikov, S. V., Shibano, Y. A., Mennickent, R. E., et al. 2004, *A&A*, 417, 1017
- Zharikov, S. V., Shibano, Y. A., Koptsevich, A. B., et al. 2002, *A&A*, 394, 633